(2)

ARMY RESEARCH LABORATORY

Cross-Barrel Temperature Difference Due to Wall Thickness Variation

Nathan Gerber
Mark L. Bundy

ARL-TR-100 March 1993

NOTICES

Destroy this report when it is no longer needed. DO NOT return it to the originator.

Additional copies of this report may be obtained from the National Technical Information Service, U.S. Department of Commerce, 5285 Port Royal Road, Springfield, VA 22161.

The findings of this report are not to be construed as an official Department of the Army position, unless so designated by other authorized documents.

The use of trade names or manufacturers' names in this report does not constitute indorsement of any commercial product.

REPORT DOCUMENTATION PAGE

Form Approved
OMB No. 0704-0188

1. AGENCY USE ONLY (Leave blank)	2. REPORT DATE	3. REPORT TYPE AND DATES COVERED
	March 1993	Final, June 91–July 92

4. TITLE AND SUBTITLE
Cross-Barrel Temperature Difference Due to Wall Thickness Variation

5. FUNDING NUMBERS
PR: 1L162618AH80

6. AUTHOR(S)
Nathan Gerber and Mark L. Bundy

7. PERFORMING ORGANIZATION NAME(S) AND ADDRESS(ES)
U.S. Army Research Laboratory
ATTN: AMSRL-WT-PB
Aberdeen Proving Ground, MD 21005-5066

8. PERFORMING ORGANIZATION REPORT NUMBER

9. SPONSORING/MONITORING AGENCY NAME(S) AND ADDRESS(ES)
U.S. Army Research Laboratory
ATTN: AMSRL-OP-CI-B (Tech Lib)
Aberdeen Proving Ground, MD 21005-5066

10. SPONSORING/MONITORING AGENCY REPORT NUMBER
ARL-TR-100

11. SUPPLEMENTARY NOTES

12a. DISTRIBUTION/AVAILABILITY STATEMENT
Approved for public release; distribution is unlimited.

12b. DISTRIBUTION CODE

13. ABSTRACT *(Maximum 200 words)*

Advances in manufacturing techniques have reduced, but not eliminated, cross-barrel wall thickness variation in the production of gun barrels. Structurally, these small variations will not appreciably diminish the strength of the barrel, and are, therefore, not a firing safety concern. However, even small variations will produce cross-barrel temperature differences that can increase with the number of rounds fired, and thereby produce thermal distortion of the barrel, which degrades gun accuracy. This investigation presents a theoretical (finite difference) analysis of the cross-barrel temperature difference expected to occur as a result of typical and atypical wall thickness variation in production-line guns. The results indicate that typical barrels will not incur an appreciable thermal bend due to wall thickness variation. However, current manufacturing tolerances would allow an atypical barrel to be fielded that could undergo significant thermal distortion due to a cross-barrel temperature difference created by asymmetric wall thickness.

14. SUBJECT TERMS
gun barrel heating, finite difference theory, wall thickness variation, cross-barrel temperature difference, M256 120-mm gun barrel, repeated firing, gun barrels

15. NUMBER OF PAGES
50

16. PRICE CODE

17. SECURITY CLASSIFICATION OF REPORT	18. SECURITY CLASSIFICATION OF THIS PAGE	19. SECURITY CLASSIFICATION OF ABSTRACT	20. LIMITATION OF ABSTRACT
UNCLASSIFIED	UNCLASSIFIED	UNCLASSIFIED	UL

INTENTIONALLY LEFT BLANK.

TABLE OF CONTENTS

INTENTIONALLY LEFT BLANK.

LIST OF FIGURES

INTENTIONALLY LEFT BLANK.

ACKNOWLEDGMENTS

The authors would like to thank the following U.S. Army Research Laboratory* (ARL) co-workers: James Bradley (PFD) for programming the finite-difference solution; John Petresky (contractor) for his help in getting the program to run on the ARL supercomputer; Emily Hsi (contractor) for graphical sketches; and Paul Conroy and George Keller (PFD) for interior ballistics input and funding, respectively. They would also like to thank Britt Overocker, Watervliet Arsenal, for his input on the gun manufacturing process.

* Note: The U.S. Army Ballistic Research Laboratory (BRL) was deactivated on 30 September 1992 and subsequently became a part of ARL on 1 October 1992.

INTENTIONALLY LEFT BLANK.

1. INTRODUCTION

Outwardly, gun barrels appear axially symmetric. Yet, when a gun is fired, the barrel temperature rise is typically not axisymmetric. For instance, instead of the temperature rising uniformly at a given axial location, firing may elevate the barrel temperature more on the left side than on the right in one area, and more on the bottom than the top in another area, or vice versa. Any cross-barrel temperature difference (CBTD) will produce a cross-barrel thermal expansion difference that causes off-axis bending of the barrel during firing. This thermal bending/distortion decreases tank gun accuracy and is, therefore, a situation to be avoided. (The CBTD referred to here, ΔT_o, is defined as the difference between the temperatures at the two intersection points on the outer wall of the barrel formed by a line in the transverse plane passing through the center of the bore. A similar CBTD for the inner wall, ΔT_i, will be introduced later. The difference between the lengths of the two segments between inner and outer walls formed by this same line is called the "wall thickness variation.")

The terms "bore centerline" (or "centerline") and "centerline deviation" are now introduced. Consider an infinite set of planes intersecting the gun barrel so that the inner wall forms a circle in each plane. Then the locus of the centers of these circles is the three-dimensional centerline curve. When there is no bending of the gun tube, the centerline is straight, coinciding with the rotation axis of the machining tool. In a given longitudinal plane through the rotation axis, the centerline trace is a curve that deviates slightly from the rotation axis; the amount of displacement (normal to the rotation axis) is the centerline deviation.

The source of CBTD has long been a topic of discussion/speculation (Manaker and Croteau 1976; Bundy 1987a, 1987b). For example, in the case-study of Bundy (1987b), test results indicated a possible correlation between CBTD and the centerline deviation. (In a plane passing through the rotation axis, the temperature rise was generally greater on the same side of the rotation axis as the centerline deviation.) Apparent correlations and speculations aside, we shall show that wall thickness variation will indeed produce CBTD.

To predict the CBTD due to wall thickness variation during firing, we shall solve the time-dependent, two-dimensional (radial and circumferential) equations that govern heat transfer

into, through, and out of the gun barrel by the method of finite differences. Primarily, results will be computed for a specific, but typical, production-line M256 120-mm gun barrel and for a service-acceptable, yet atypical, production-line barrel.

To provide some understanding of the origins of wall thickness variation, we shall briefly describe the gun barrel manufacturing process. It will become apparent that wall thickness variation and centerline deviation are related, to some degree, as a consequence of the manufacturing process. Thus, the apparent correlation noted by Bundy (1987b) between CBTD and centerline deviation may—more fundamentally—be a correlation between CBTD and wall thickness variation.

2. THE GUN BARREL MANUFACTURING PROCESS

Much effort has been devoted in the manufacturing process of large-caliber guns to minimizing lateral wall thickness variation. In general, circularity of the inner and outer surface is not the problem—concentricity is. That is, wall thickness variation is caused primarily by the non-alignment of the axes of rotation of the inner and outer surfaces of revolution during their machining. It is conjectured that this comes about as follows.

After removal from the forge and heat treatment (to relieve residual forging stress), the barrel is ready to be "finished" (a multistep process to bring the rough forged barrel to its final design/drawing specifications). The inner surface is finished first, which means that it is bored, honed, swaged, and thermally treated to help relieve swaging stress, then bored again, and honed again. It has a relatively straight centerline before finishing work is begun on the outer surface. Initially, the axis of rotation for machining the outer surface is the same as the axis of the inner surface (i.e., the bore centerline, see Figure 1a). However, when metal is removed by turning down the outer surface, it relieves non-uniform residual swaging stress, which causes the barrel to "spring" or bend off-axis. Whenever and wherever this happens during machining, it misaligns the bore centerline from the rotational axis of the yet-to-be finished outer surface, and thus produces both lateral wall thickness variation and bore centerline deviation in the gun barrel. As illustrated in Figure 1b, the wall thickness variation will be twice the centerline deviation at—and only at—the place where material is being cut,

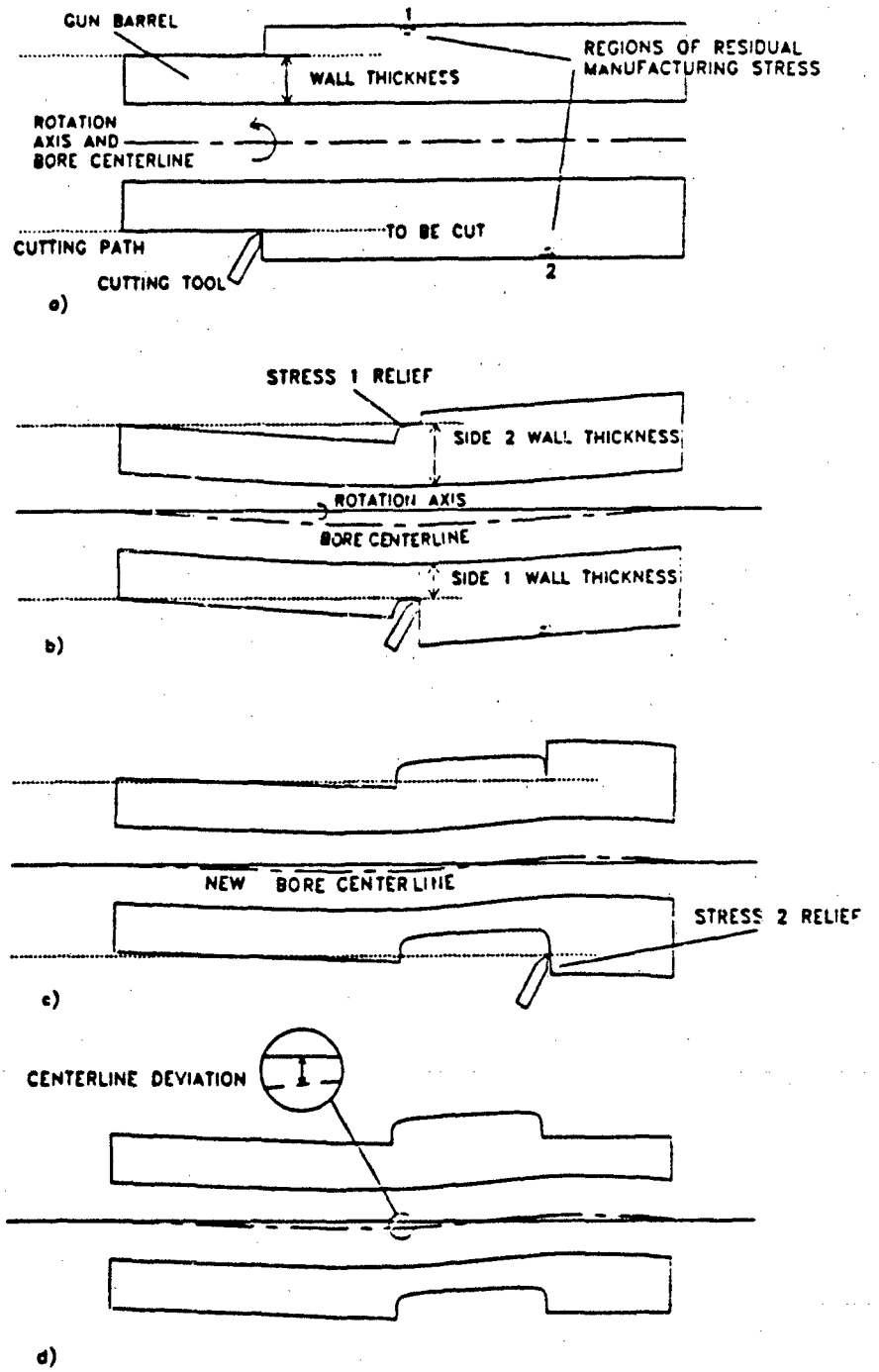

Figure 1. Schematic representation of outer-wall gun barrel machining, a) before and b)–d) after "springing" due to residual stress relief caused by removal of material from the outer wall.

since stress relief at a new cut site will change the centerline deviation everywhere along the barrel including previous cut sites (Figure 1c). Furthermore, it is common practice to attempt to mechanically straighten a gun barrel (with a hydraulic press) during or after machining. Nevertheless, we might expect that some residual correlation between centerline deviation and wall thickness variation will remain along the finished barrel, as illustrated in Figure 1d.

In Figures 2 and 3 we have plotted the centerline deviation and wall thickness variation along the bore for a typical production-line M256 gun tube, serial number 4251. Due to the limitations of the centerline measurement technique, the centerline deviation is plotted relative to the line joining its two end measurements. To be consistent, we have likewise plotted the wall thickness variation relative to its two end measurements. Clearly, centerline deviation and wall thickness variation are not correlated by the simple 2:1 ratio indicated in Figure 1b (where stress is relieved at only one location along the barrel), yet the two factors do tend to oppose each other in a fashion consistent with Figure 1d (where stress has been relieved at multiple locations). That is, the wall thickness variation is generally positive where the centerline deviation is negative (see Figures 2 and 3), which implies the thinner wall is on the same side of the axis of rotation as the centerline deviation.

Lastly, in the manufacturing process, the outer surface is ground slightly (while turning), followed by chrome plating of the inner surface. These finishing steps can also change the wall thickness variation and the centerline curvature, but the change is usually less than 25%.

For the M256 gun barrel, specifications (McDermott 1991) call for the wall thickness variation to be no more than 1.5 mm over most of the barrel (with the exception of the chamber area, which has closer tolerances). In actuality, however, most M256 barrels are manufactured, like serial number 4251 (Figures 2 and 3), with less than 0.5 mm wall thickness variation (Overocker 1991).

A wall thickness variation of 1.5 mm will correspond to less than 10% of the total wall thickness, depending on the location along the barrel. However, such a wall thickness variation will produce an equivalent variation in the temperature rise between one side and the

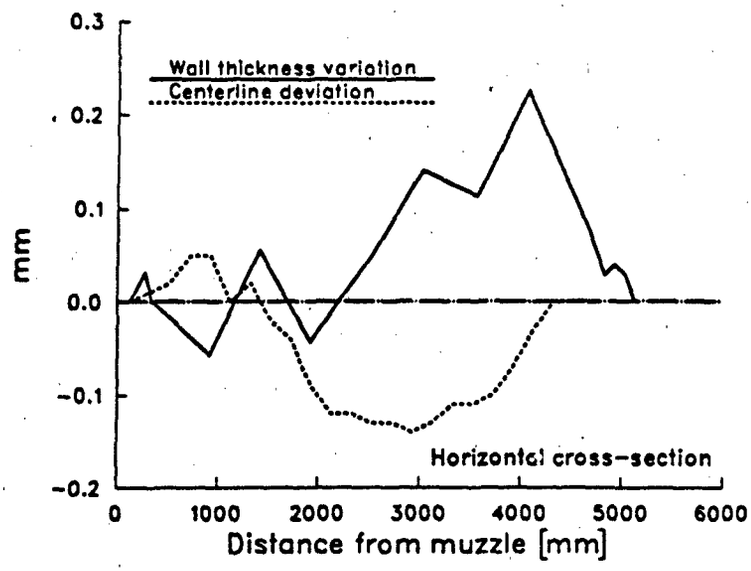

Figure 2. Centerline deviation and wall thickness variation (right side minus left) for an M256 barrel, serial number 4251.

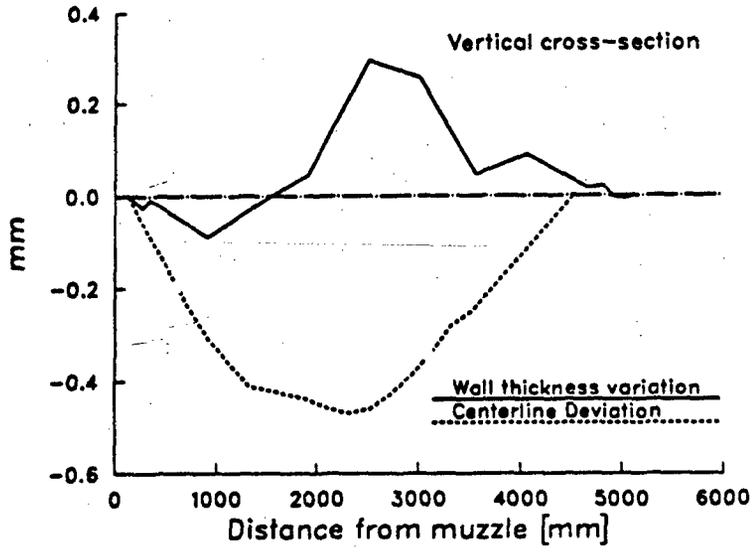

Figure 3. Centerline deviation and wall thickness variation (top minus bottom) for an M256 barrel, serial number 4251.

other. For instance, if the nominal barrel temperature rise from firing a round is 10° C at a location where the wall thickness varies by 10% between one side and the other, then the CBTD will be approximately 1° C at this site. This CBTD will increase if the gun is fired rapidly. For reference, Bundy (1987b) showed that a 2° to 3° C change in the CBTD over a relatively short length of the barrel (<1 m) will produce a muzzle angle change of several tenths of a miliradian. We shall show that almost any "fast" rate of fire will yield a CBTD of several degrees if the wall thickness variation approaches the maximum allowed by current manufacturing guidelines.

3. THE HEATING MODEL

We shall compute the CBTD for multiple firings by employing an extension of the model used in Gerber and Bundy (1991). The following assumptions apply here:

(1) Temperature gradients in the longitudinal direction are neglected in comparison with those in the radial direction. (The longitudinal axis is taken to be a locally straight segment at the transverse plane under consideration.)

(2) Axisymmetric heat input is assumed, and gravity effects in the cooling process are neglected.

(3) Feedback of barrel heat to flow in the gun bore is neglected, so that the same bore temperature and convective heat transfer coefficient histories (for a single round) furnish the input data for every round calculated.

(4) Friction heating is neglected.

(5) Thermal expansion of the barrel is not considered to have an effect on the heat transfer process.

(6) The thermal conductivity, k, the specific heat, c_p, and the density, ρ, of the metal are constants (see Chapter 5).

(7) The offset distance (ε) between the axes of the inner and outer walls is very small compared to the radii of the walls themselves. For example, in the extreme case for the M256 120-mm gun, the axes displacement would be less than 1 mm, while the inner radius of the barrel would be at least 60 mm.

4. FORMULATION OF THE PROBLEM

4.1 Statement of Problem. We state our problem in terms of cylindrical coordinates r, ϕ, and z. Figures 4a and 4b show the transverse plane viewed from the muzzle. The axial coordinate z is taken to be zero at the gun's breech (Figure 4c). The z-axis coincides with the centerline of the bore (i.e., the axis of the inner wall surface), which intersects the r, ϕ plane at the origin, O. (Note, the right-handed coordinate system that we have chosen is consistent with the reference system of most interior ballistics models. However, it differs from the so-called gunner's coordinate system, which chooses the positive x-axis to lie on the gunner's right, which is our negative x-axis.) The radii of the inner and outer walls, referenced to their individual axes of rotation, are R_i and R_o, respectively. In our model we assume that the axis of the outer wall is displaced to the right of the axis of the inner wall by a distance ε to simulate the imperfection of manufacture. The radius of the outer wall relative to the origin will be designated by $r = r_o(\phi)$.

At a given axial location, z, the gun barrel temperature, $T(r,\phi,t)$, is determined by the following differential equation of heat conduction for a stationary, homogeneous, isotropic solid with no internal heat generation (Holman 1981, p.6):

$$\partial^2 T/\partial r^2 + (1/r)\,\partial T/\partial r + (1/r^2)\partial^2 T/\partial \phi^2 = (1/\alpha)\partial T/\partial t, \qquad (1)$$

where t = time from the initiation of the first round. The constant $\alpha \equiv k/(\rho\, c_p)$ is the thermal diffusivity.

Let T_∞ designate the ambient temperature of the atmosphere (assumed to be constant). Then the initial condition is

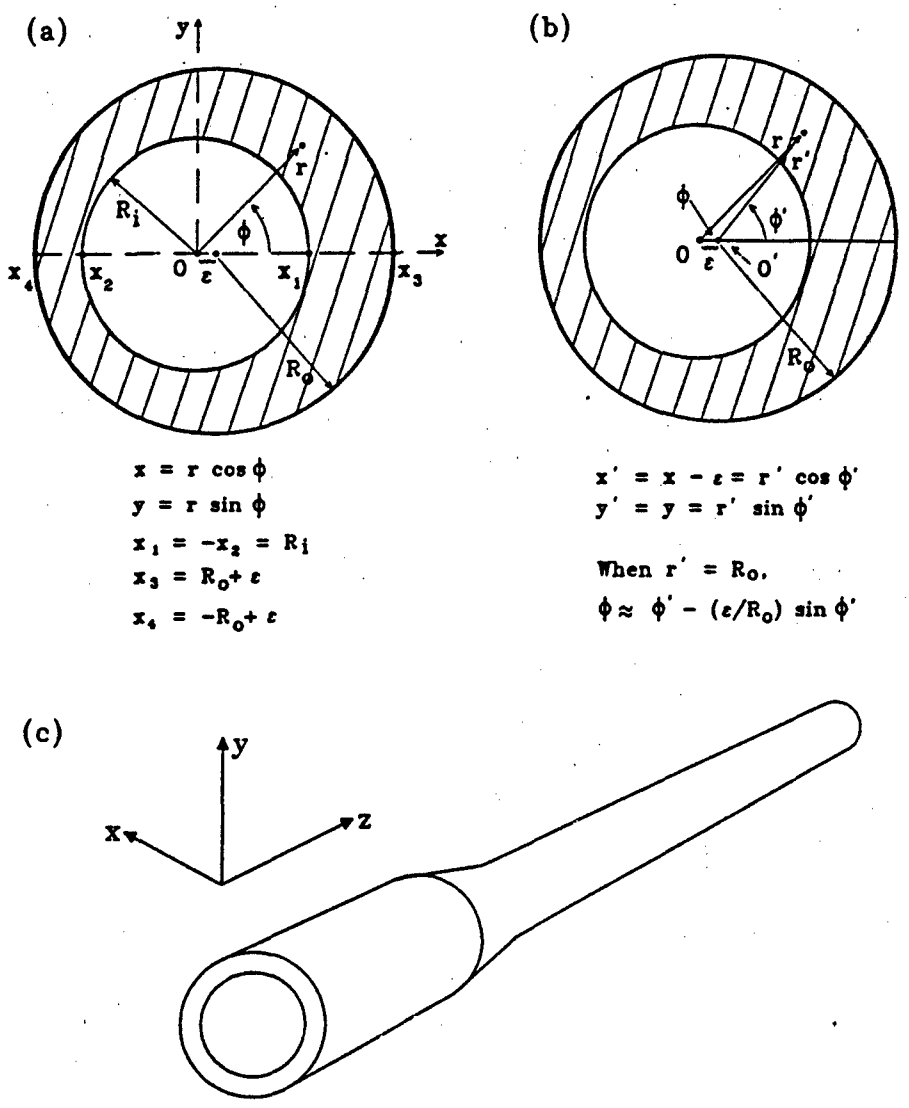

Figure 4. Transverse cross section of a gun barrel of nonuniform thickness, viewed in a) and b) from the muzzle, and in c) from an oblique angle of the breech.

$$T(r,\phi) = T_\infty \qquad t = 0, \quad R_i \le r \le r_o(\phi) \quad (z = const). \tag{2}$$

The boundary conditions at the inner and outer walls are obtained by Newton's law of cooling (see, e.g., Özisik [1968]). The axisymmetric boundary condition at the inner wall is

$$k\,\partial T/\partial r - h_g T = -h_g T_g \qquad r = R_i, t>0 \ (z = const), \tag{3}$$

where $T_g(t,z)$ is the cross-sectional average temperature of the flow in the bore, and $h_g(t,z)$ is the coefficient of heat transfer between the gas-particle mixture in the bore and the inner wall of the barrel. $T_g(t,z)$ and $h_g(t,z)$ are known from interior ballistic computations and thus constitute input.

The outer wall boundary condition introduces azimuthal variation into the problem. The outer wall equation is

$$r_o = [R_o^2 - \varepsilon^2 \sin^2\phi]^{1/2} + \varepsilon\cos\phi\,.$$

We restate one of the basic assumptions,

$$\varepsilon << R_i, R_o \tag{4}$$

and retain only terms through <u>first order in ε</u>. Then for the outer wall,

$$r_o = R_o + \varepsilon\cos\phi\ . \tag{5}$$

The boundary condition here, which includes both <u>convective</u> and <u>radiative</u> cooling (Özisik 1968, Equations 1–28 and 8–137c; Gerber and Bundy 1992, Equation 4), is

$$-k\,\partial T/\partial n = h_\infty(T-T_\infty) + F\sigma(T^4 - T_\infty^4) \qquad r = r_o\,, t > 0 \ (z = const), \tag{6}$$

where $\partial T/\partial n$ is the component of grad T normal to the barrel surface, and $h_\infty = h_\infty(z)$ is the coefficient of convective heat transfer between the barrel wall and the surrounding

atmosphere. F is the radiation interchange factor between the barrel outer wall and the environment (in our case, we assume $F = 0.95$), and σ is the Stefan-Boltzmann constant [$= 5.669 \times 10^{-8}$ $J/(m^2\ s\ K^4)$].

A unit outward vector normal to the outer wall (correct through $O(\varepsilon)$) is $\underline{U}_n = [1, \varepsilon(1/r)\sin\phi]$; grad $T = [\partial T/\partial r, (1/r)\,\partial T/\partial\phi]$. Then, $\partial T/\partial n = \underline{U}_n \cdot$ grad T in Equation 6. On the line $r = R_o + \varepsilon\cos\phi$, Equation 6 becomes

$$-k\,[\partial T/\partial r + (\varepsilon/r^2)\sin\phi\ \partial T/\partial\phi] = h_\infty(T - T_\infty) + F\sigma(T^4 - T_\infty^4) \qquad (7)$$

Applying the expansion

$$F_n(r = R_o + \varepsilon\cos\phi) = F_n(R_o) + (\partial F_n/\partial r)_{R_o}\varepsilon\cos\phi + O(\varepsilon^2)\ ,$$

(where F_n is any function of r) to Equation 7 leads to

$$-k\left[\frac{\partial T}{\partial r} + \left(\frac{\partial^2 T}{\partial r^2}\right)\varepsilon\cos\phi + \frac{\varepsilon}{R_o^2}\sin\phi\left(\frac{\partial T}{\partial\phi}\right)\right] = h_\infty\left[T - T_\infty + \varepsilon\cos\phi\left(\frac{\partial T}{\partial r}\right)\right] +$$

$$F\sigma\left[T^4 - T_\infty^4 + 4\varepsilon T^3(\partial T/\partial r)\cos\phi\right] + O(\varepsilon^2) \qquad \text{at } r = R_o\ . \qquad (8)$$

To retain linearity in the outer wall boundary condition, we apply the reasonable approximation that $|T^{m+1} - T^m| << T^m$ at $r = R_o$. Here the superscript $m + 1$ refers to the current time step of calculation, while m denotes the immediately preceding time step when T is known. Thus,

$$(T_{NI+1}^{m+1})^4 = 4(T_{NI+1}^{m})^3\ T_{NI+1}^{m+1} - 3(T_{NI+1}^{m})^4\ ,$$

which is linear in T_{NI+1}^{m+1}. The subscript $NI + 1$ denotes $r = R_o$.

4.2 Special Form of Solution. When a solution of the form*

$$T = T_1(r,t) + \varepsilon \cos\phi \; T_3(r,t) \tag{9}$$

is substituted into Equations 1, 2, 3, and 8, the 2-D problem is reduced to two one-dimensional (1-D) problems by collecting terms for each power of $\varepsilon \cos \phi$. The statements of these two problems now follow:

$$(1/\alpha)\,\partial T_1/\partial t = \partial^2 T_1/\partial r^2 + (1/r)\,\partial T_1/\partial r \tag{10a}$$

$$T_1(r,t) = T_\infty \qquad t = 0,\ R_i \le r \le R_o \tag{10b}$$

$$k\,\partial T_1/\partial r = h_g(T_1 - T_g) \qquad r = R_i,\ t > 0 \tag{10c}$$

$$k\,\partial T_1/\partial r + [h_\infty + 4F\sigma(T_1^m)^3]T_1 = h_\infty T_\infty + F\sigma[T_\infty^4 + 3(T_1^m)^4]$$

$$r = R_o,\ t > 0, \tag{10d}$$

and

$$(1/\alpha)\,\partial T_3/\partial t = \partial^2 T_3/\partial r^2 + (1/r)\,\partial T_3/\partial r - (1/r^2)\,T_3 \tag{11a}$$

$$T_3(r,t) = 0 \qquad t = 0,\ R_i \le r \le R_o \tag{11b}$$

$$k\ \partial T_3/\partial r = h_g\ T_3 \qquad r = R_i,\ t > 0 \tag{11c}$$

$$\partial T_3/\partial r + (h_\infty + 4F\sigma T_1^3)\,T_3/k = W(T_1) \qquad r = R_o,\ t > 0, \tag{11d}$$

where

---

* The choice of T_3 instead of T_2 for the perturbation was made to maintain consistency with the nomenclature of the computer program.

$$W(T_1) \equiv -\partial^2 T_1 / \partial r^2 - (h_\infty + 4F\sigma T_1^3)(\partial T_1 / \partial r)/k$$

$$r = R_o,\ t = t^{m+1}. \qquad (12)$$

The first problem is the axisymmetric problem previously solved (Gerber and Bundy 1991, 1992). The second problem is coupled to the first through the outer wall boundary condition (Equation 11d). The function $W(T_1)$ is a known quantity at the time of solution, so that the two problems can be solved in tandem.

4.3 Transformed Radial Coordinate. We introduce a transformation, as in Gerber and Bundy (1991, 1992),

$$r = r(\xi) \qquad (0 \le \xi \le 1), \qquad (13)$$

so that the constant increment $\Delta\xi$ will cluster the nodal points closely together near the inner wall, where $T_1(r,t)$ gradients are largest, and spread them out away from there. We define the transformation in the following two steps:

$$\zeta(\xi) = \gamma\xi + (1-\gamma)\xi^\beta \qquad (0 < \gamma \le 1,\ \beta > 2), \qquad r = D\zeta + R_i, \qquad (14)$$

where $D \equiv R_o - R_i$, and γ and β are chosen constants. We have used $\gamma = 0.092$, $\beta = 2.25$. Note that $r = R_i$, R_o correspond to $\xi = 0$, 1, respectively. The actual computations are then carried out in the (ξ, t) space; a restatement of the problems in ξ and t is provided in Appendix A.

4.4 Wall Temperatures. The wall temperatures are of particular interest, especially that of the outer wall, which is the most easily measurable. At the inner wall,

$$T_i \equiv T(r = R_i) = T_1(R_i,t) + \varepsilon\cos\phi\ T_3(R_i,t). \qquad (15)$$

At the outer wall,

$$T_o \equiv T(r = R_o + \varepsilon\cos\phi) = T_1(R_o,t) + \varepsilon\cos\phi\ [\partial T_1/\partial r + T_3]_{r=R_o}, \qquad (16)$$

where $(\partial T_1/\partial r)$ at $r = R_o$ is given by Equation 10d (or Equation B-11a).

A diameter cutting across the gun barrel is properly described by the angles $\phi' = \phi_1'$ and $\phi' = \phi_1' + \pi$ (see Figure 4b). Since $\phi = \phi' + O(\varepsilon)$ (Figure 4b), ϕ may be replaced by ϕ' in Equations 15 and 16 without changing the accuracy of the approximation.

Equation 9 indicates that the entire azimuthal variation of temperature is contained in the cos ϕ factor. Since $T_3(r, t) \leq 0$ in Figure 5, Equations 15 and 16 show that T_i and T_o vary from a maximum at $\phi = \pi$ to a minimum at $\phi = 0$.* The maximum changes in temperature across the diameters of the inner and outer walls are, respectively,

$$\Delta T_i \equiv T_i(\phi = \pi) - T_i(\phi = 0) = -2\,\varepsilon\, T_3(R_i, t) \tag{17a}$$

$$\Delta T_o \equiv T_o(\phi = \pi) - T_o(\phi = 0) = -2\varepsilon\,[T_3 + \partial T_1 / \partial r]_{r = R_o} \,. \tag{17b}$$

Calculations indicate that generally $|(\partial T_1 / \partial r) / T_3|_{R_o} \leq 0.005$, so that

$$\Delta T_o \equiv -2\varepsilon\, T_3(R_o, t) \,.$$

Thus, at a given station, z, for a particular round, the maximum CBTDs are proportional to ε, to the order of our approximation.

5. INPUT DATA

A detailed discussion of the input to the computations is given in Gerber and Bundy (1991). Briefly, however, T_g is computed at chosen stations along the bore from the NOVA code (Gough 1980) and h_g is computed from the Veritay code (Chandra and Fisher 1989a, 1989b), which uses T_g and other NOVA variables to determine h_g by the method of Stratford and Beavers (1961).

* T_3 can actually become positive late in a long cooling cycle (see Chapter 7).

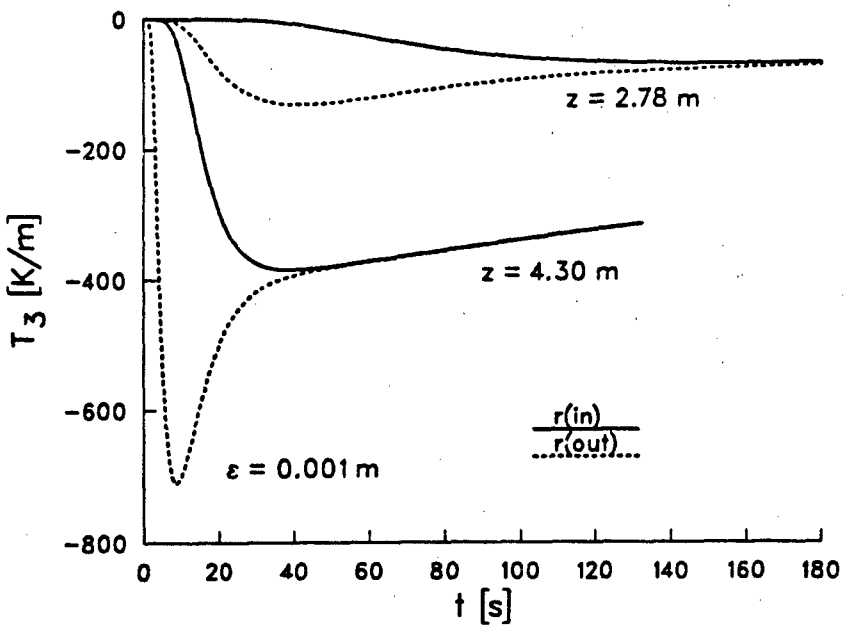

Figure 5. Single-round histories of T_3 at inner and outer walls at two axial stations.

Figures 6a and 6b show representative T_g and h_g histories at two stations on an M256 120-mm gun barrel. It is seen that T_g and h_g remain constant until the base of the projectile passes the given station at time $t = t_d$. At this time, these variables rise suddenly, then they decrease more gradually with h_g decaying significantly faster than T_g.

All the computations reported here were performed for the case of an M256 120-mm tank gun firing a DM13 round.* However, the results are not expected to change significantly for other round types. The values of properties of the gun barrel metal are taken to be

$$c_p = 469.05 \ J/(kg \ \ K)$$

$$k = 38.07 \ J/(m \ s \ K)$$

$$\rho = 7{,}827.0 \ kg/m^3 \ .$$

* Table I of Gerber and Bundy (1991) describes the shape and size of the gun barrel.

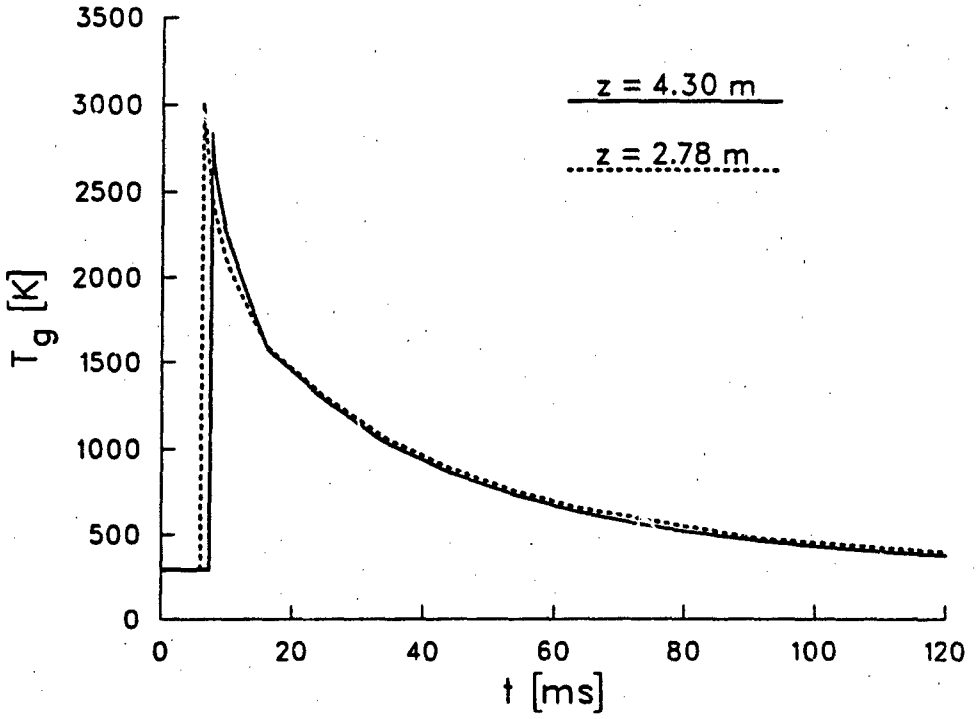

Figure 6a. Bore gas temperature histories at two axial stations.

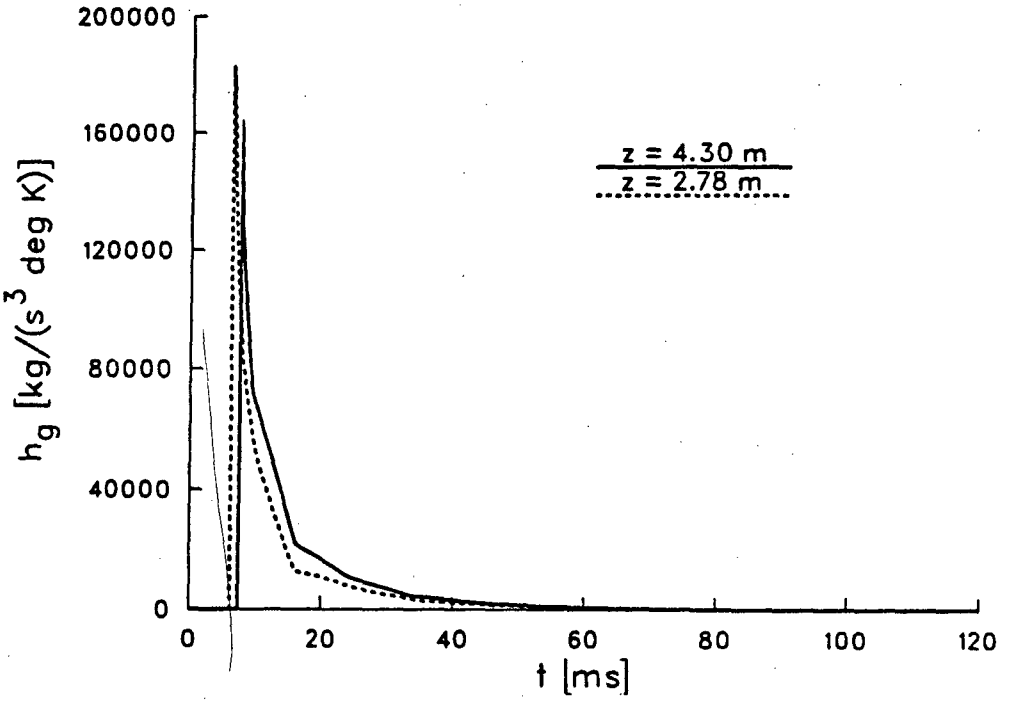

Figure 6b. Convective heat transfer coefficient histories at inner wall of gun barrel at two axial stations.

The diffusivity is thus

$$\alpha = 1.03698 \times 10^{-5} \ m^2/s .$$

The ambient condition constants are

$$T_\infty = 294.4 \ \ K \ \text{(unless otherwise stated)}$$

$$h_\infty = 6.0 \ \ kg/(s^3 \ K) .$$

The above value of c_p was measured in 1990 by Joseph Cox, Benet Weapons Laboratory, for M256 gun barrel steel (assumed to be ASI 4340) at 295 K. The values for k and ρ were obtained from Talley (1989) for 4335 steel. The value for h_∞ was obtained from experiments conducted by Bundy on a shrouded M256 barrel.

6. FINITE-DIFFERENCE CALCULATION

For the finite-difference calculations, the interval $0 \le \xi \le 1$ (corresponding to $R_i \le r \le R_o$) is divided by equally spaced nodal (or grid) points into NI subintervals. The constant ξ increment is $\Delta\xi = 1/NI$, and location of the nodes is given by $\xi_j = (j - 1)\ \Delta\xi$ ($j = 1, 2, \ldots NI+1$). Derivatives at node j are approximated as follows (for $H = T_1, T_3$):

$$(\partial H/\partial\xi)_j = (-3 H_j + 4H_{j+1} - H_{j+2})/(2\ \Delta\xi) \quad (j=1) \tag{18a}$$

$$(\partial H/\partial\xi)_j = (H_{j+1} - H_{j-1})/(2\ \Delta\xi) \quad (j = 2, \ldots, NI) \tag{18b}$$

$$(\partial H/\partial\xi)_j = (H_{j-2} - 4H_{j-1} + 3H_j)/(2\ \Delta\xi) \quad (j = NI+1) \tag{18c}$$

$$(\partial^2 H/\partial\xi^2)_j = (H_{j-1} - 2H_j + H_{j+1})/(\Delta\xi)^2 \quad (j = 2, \ldots, NI) . \tag{18d}$$

If we let the time increment be $\Delta t = t^{m+1} - t^m$, then, in the Crank-Nicolson scheme employed here (Özisik 1968, p. 402) to obtain the solution at time $t = t^{m+1}$,

$$(1/2)\left[(\partial H/\partial t)_t m + (\partial H/\partial t)_t m+1\right] = (H^{m+1} - H^m)/\Delta t. \qquad (19)$$

The finite difference approximations to the equations and boundary conditions are produced by substituting the derivative approximations of Equations 18 and 19 into Equations A-4 and A-5, and then collecting terms. After some labor, one obtains the following two sets of linear equations for $T_{1_n}^{m+1}$ and $T_{3_n}^{m+1}$:

$$\sum_{n=1}^{NI+1} A_{jn}\, T_{1_n}^{m+1} = d_j \qquad (J = 1,2,\ldots NI+1) \qquad (20)$$

$$\sum_{n=1}^{NI+1} B_{jn} T_{3_n}^{m+1} = e_j \qquad (j = 1,2,\ldots NI+1). \qquad (21)$$

The coefficients A_{jn}, B_{jn}, d_j, and e_j are given in Appendix B. The d_j's and e_j's involve T_1 and T_3 values calculated for the previous timestep $t = t^m$. A standard FORTRAN routine is applied to solve Equations 20 and 21; in most cases, we have used $NI = 100$.

There are essentially two time scales in the present problem: 1) the duration of the firing (roughly 100 ms) and 2) t_f, the time between firings (usually 5 seconds or more when firing large guns). The Δt should be sufficiently small to resolve the phenomenon in case 1 but should be larger in case 2 to save time in computation. The program contains a subroutine prescribing Δt as a function of t within a firing cycle (see Appendix C).

The coefficients in the heat conduction equation and boundary conditions are known functions of t. Thus, only a single iteration is required to obtain the solution to the finite-difference equations. The Crank-Nicolson method is stable for all values of Δt, and there are no restrictions on the relative sizes of Δt and $\Delta\xi$.

7. COMPUTATIONS

We apply our numerical simulation to an investigation of the nonaxisymmetric barrel temperature resulting from an imperfect alignment of inner and outer wall barrel axes in an M256 120-mm gun. Most of the CBTD plots that follow are shown for $\varepsilon = 1$ mm. The CBTD for any other displacement is readily obtained from these plots by multiplying the temperature difference values by ε in millimeters, since ΔT_i and ΔT_o are both proportional to ε (Equation 17).

First, we show results for a single round. Figure 7 presents unperturbed (axisymmetric) barrel temperature histories, T_1, while Figure 5 includes the variation of the perturbation function, T_3, at the same location. In both instances, the functions tend to approach constant values across the barrel in finite umes, as evidenced by the coalescing of the curves for the inner and outer walls. The time for the radial equilibration of T_1 was referred to as the outer-wall rise time, t_r, in Gerber and Bundy (1991). For consistency, we shall continue to use this designation here. Furthermore, we shall refer to the radial equilibration time of T_3 as the rise time t_{r3}. There is no exact criterion for defining rise time; an estimate can be made on the basis of inspection of the curves. For the example shown in Figures 5 and 7, t_{r3} is considerably larger then t_r. The *cos* ϕ factors in Equations 15 and 16 prevent circumferential equilibration as long as T_3 is non-zero. In Figure 5, T_3 appears to approach zero with time.

Next, we consider constant rate-of-fire. The first example (at $z = 4.30$ m) deals with slow rate-of-fire (i.e., t_r and $t_{r3} < t_f$, where t_f is the time interval between successive rounds). Here $t_f = 60$ s, $t_r \approx 26$ s, and $t_{r3} \approx 45$ s. Rise times are essentially independent of number of rounds fired, but they depend on local barrel thickness. Figure 8 shows T_1, the symmetric part of T, at the inner and outer walls as functions of time. The upward-facing spikes for the inner wall represent the rapid rise in temperature produced at the time of firing; the succeeding rapid decline occurs when heat input stops and heat is conducted into the interior of the barrel. It is seen that T_1 (R_o) lags behind T_1 (R_i) in each cycle in the rise from its pre-firing value. This lag is a consequence of the time required for a significant effect of the thermal disturbance applied at the inner wall to reach the outer wall.

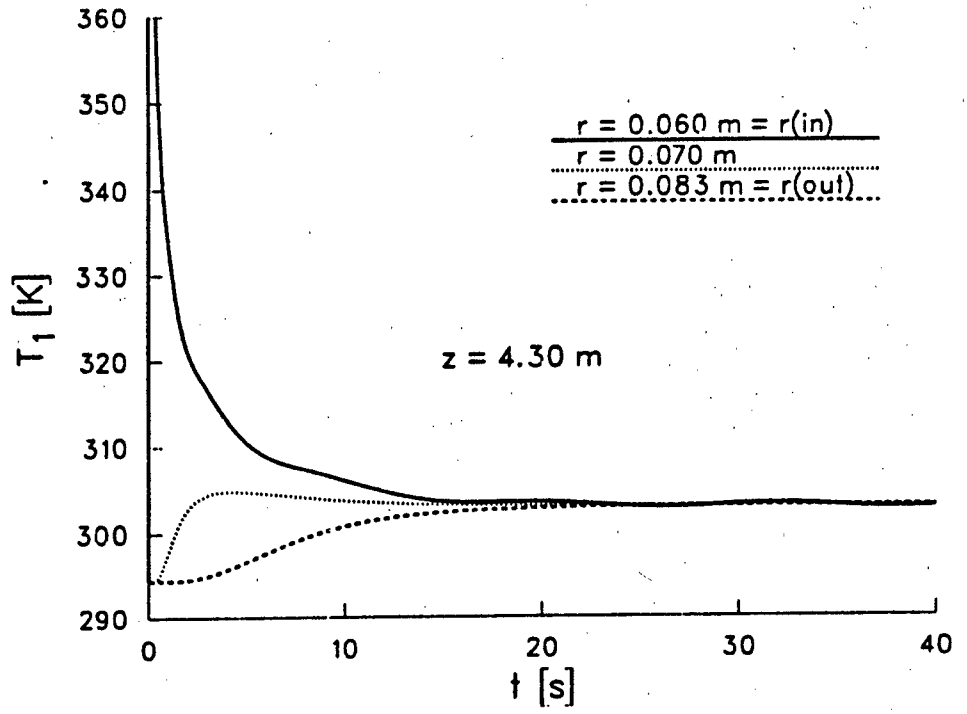

Figure 7. Single-round histories of unperturbed temperature, T_1, at three radial locations.

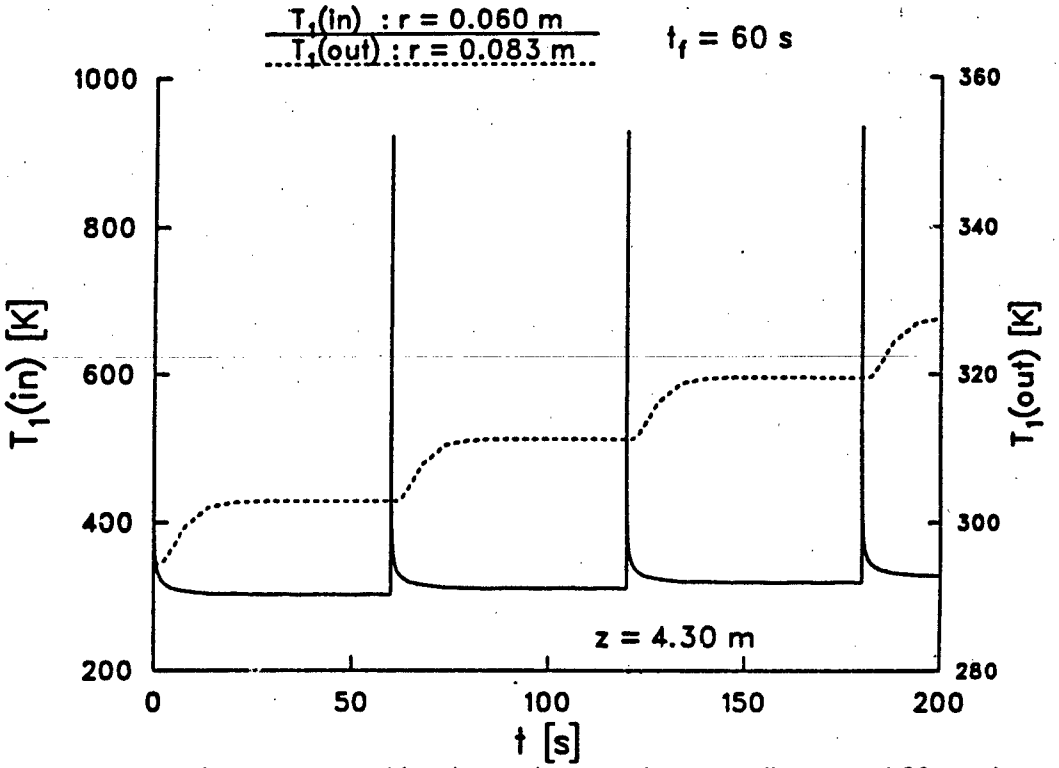

Figure 8. Axisymmetric temperature histories on inner and outer walls at z = 4.30 m, slow rate-of-fire.

Figure 9 presents the ΔT_i and ΔT_o histories for this same case. The inner and outer wall curves coincide roughly over the latter portion of each firing cycle because the firing interval is large enough so that radial equilibration is reached before the next round is fired. Except for the first round, when $\Delta T_i = \Delta T_o = 0$ prior to firing, there is a downward-facing spike at the inner wall coinciding in time with the input of heat from the combustion. This is understandable; heat flux from the bore gas to the barrel is proportional to $(T_g - T_i)$, and thus, more heat will be flowing into the thicker, cooler side, raising T_i faster there than on the thinner, hotter side. This will decrease ΔT_i for an initial period of time. However, since the cooler side is thicker, the rise in T_i will eventually be less on that side, thus accounting for the overall positive ΔT_i following the initial downward-facing spike.

For each round, the ΔT_o will begin to rise after the heat pulse from the inner wall reaches the outer wall on the thinner side (located at $x_4 = -R_o + \varepsilon$ in Figure 4). The effect of the wall thickness asymmetry is then propagated inward, and the time taken for the resulting perturbation to spread to the inner wall accounts for the lag in Figure 9 of the rise of ΔT_i behind that in ΔT_o. $T(x_4)$ and $T(x_3)$ (Figure 4) reach maxima because the energy input is finite; $\Delta T_o = T(x_4) - T(x_3)$ eventually peaks and then decreases as the barrel cools and CBTD equilibrates. At the inner wall, the heat perturbation due to the asymmetry is experienced at x_2 sooner than at x_1; $\Delta T_i \equiv T(x_2) - T(x_1)$ varies in a manner similar to that of ΔT_o, its amplitude in a firing cycle being less than or equal to ΔT_o.

Figure 10 shows inner and outer wall maximum CBTDs at $z = 4.30$ m for a fast rate-of-fire. Again, the downward-facing spikes occur on the ΔT_i curve. In this case, however, $t_f < t_{r3}$; thus, there is insufficient time during a round for the radial equilibration of T_3 to be reached. The ΔT_i does not attain a maximum, and ΔT_o always remains larger than ΔT_i.

Figure 11 shows the CBTDs at a different station, $z = 2.78$ m, where the nominal wall thickness $D = 0.050$ m, in contrast to $D = 0.023$ m at $z = 4.30$ m. Even though $t_f = 60$ s here as in Figure 9, the t_{r3} is large enough so that $t_f < t_{r3}$ and a fast rate-of-fire heating pattern results. Note that the CBTDs are much smaller at $z = 2.78$ m than at $z = 4.30$ m.

Next, we simulate an actual firing scenario (Table 1) in which there are fast and slow firing rates and cool-down periods. The gun is an M256 120-mm tank gun, serial number 4251, firing DM13 rounds. Note, this is the same gun barrel that was used earlier to illustrate

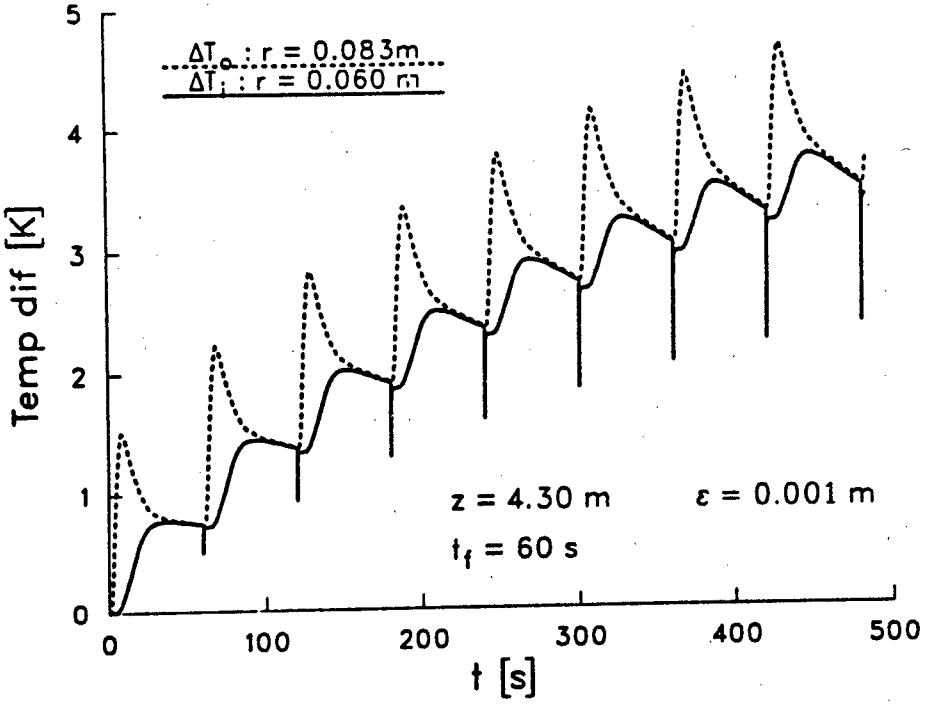

Figure 9. Histories of ΔT_i and ΔT_o at $z = 4.30$ m, slow rate-of-fire.

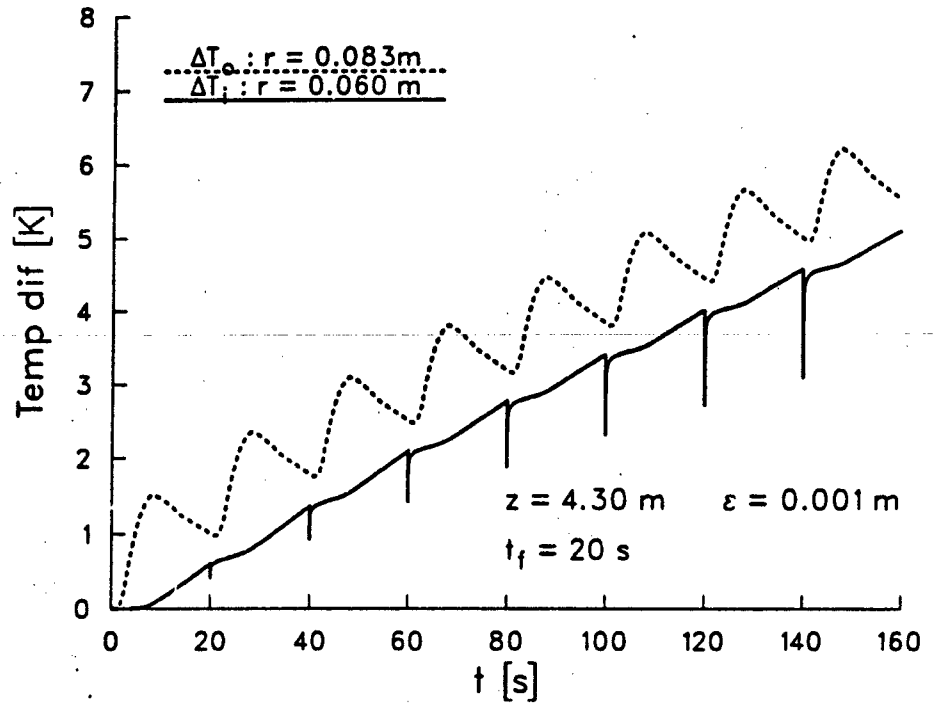

Figure 10. Histories of ΔT_i and ΔT_o at $z = 4.30$ m, fast rate-of-fire.

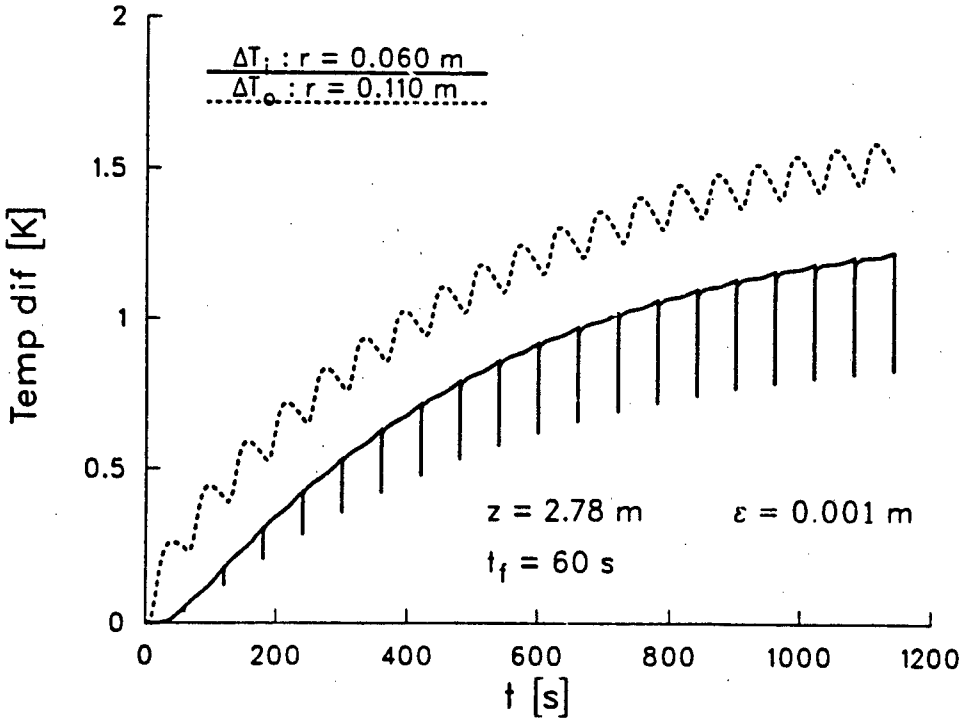

Figure 11. Histories of ΔT_i and ΔT_o at z = 2.78 m, fast rate-of-fire.

Table 1. Firing Scenario

1) 5 rounds -- t_f = 120 s	5) 10 rounds -- t_f = 36 s
2) 960 s cool-down	6) 600 s cool-down
3) 10 rounds -- t_f = 180 s	7) 4 rounds -- t_f = 180 s
4) 1,020 s cool-down	8) 600 s cool-down

(Figures 2 and 3) wall thickness variation (= 2ε) and centerline deviation for a typical M256 barrel. Table 2 shows the variation of ε (without regard to its angular orientation, ε_x and ε_y) and barrel average thickness, $D \equiv R_o - R_i$, along the gun. Figure 12 shows the inner and outer wall CBTDs computed, for example, at z = 3.950 m for the firing sequence of Table 1. For the fast- and slow-fire bursts, the curves resemble, qualitatively, corresponding plots shown in the previous figures. Radial equilibration ($\Delta T_i = \Delta T_o$) takes place early in the cooling cycles.

Table 2. Axes Separation in Test Gun

z[m]	D[mm]	ε[mm]
1.300	76.00	0.115
1.800	65.74	0.055
2.350	42.98	0.130
2.850	49.02	0.125
3.450	49.02	0.027
3.950	25.31	0.056
4.450	22.65	0.100
5.020	20.81	0.065
5.090	17.12	0.075
5.240	17.06	0.080

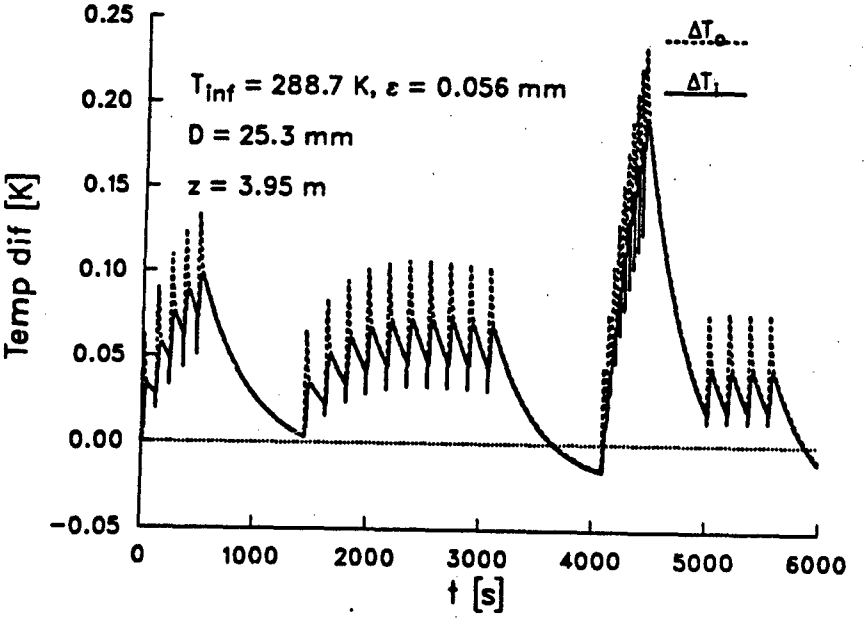

Figure 12. Histories of ΔT_i and ΔT_o at z = 3.95 m, firing scenario of Table 1, with cooling to environment.

A notable feature in Figure 12 is that ΔT_o becomes negative on two occasions ($t \cong 3{,}700$ s; 5,800 s). The physical implication here, recalling the definition of ΔT_o in Equation 17b, is that the thin side ($\pi/2 \leq \phi \leq 3\pi/2$) is originally hotter in a firing cycle than the thick side ($-\pi/2 \leq \phi \leq \pi/2$), but actually becomes cooler than the thick side later in the cycle. Basically, the reason that this happens is: at high temperatures, heat efflux from the barrel to the environment is higher than circumferential (equilibrating) heat flux within the barrel. Since the thin side has less thermal mass, its temperature drops faster from heat loss to the environment than on the thick side. Eventually, the temperature on the thin side is lower than that of the thick side, so that a reverse circumferential heat flow is required to bring about an even temperature distribution. If there were no heat loss to the surroundings, the latter phenomenon would not occur, and ΔT_o would not change sign, as is demonstrated in Figure 13.

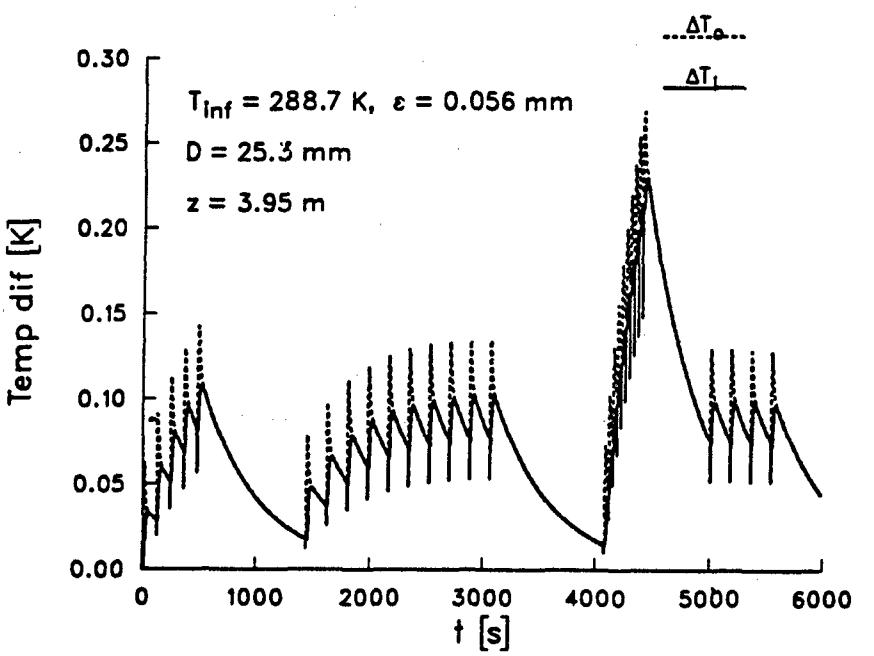

Figure 13. Histories of ΔT_i and ΔT_o at $z = 3.95$ m for an adiabatic outer wall condition, firing scenario of Table 1.

Theoretical support for the above discussion on the sign change in ΔT_o can be drawn from an approximate analysis for cool-down that yields an analytical solution to the heat transfer problem. This model, which omits radiation cooling for simplification, is outlined in Appendix D. It estimates the time of crossover of ΔT_o when there is convective cooling to the environment. It also demonstrates the absence of an undershoot without convective cooling; thus, in Equation D-10, $t_u \rightarrow \infty$ as $h_\infty \rightarrow 0$.

8. CBTD DUE TO WALL THICKNESS VARIATION IN PRODUCTION LINE M1A1 GUN BARRELS

A wall thickness variation on the order of 2 mm (ε = 1 mm) can create a substantial CBTD after repeated firings (e.g., Figure 9). However, most M256 gun barrels manufactured since the late 1980s have a wall thickness variation far below this value, as discussed in Chapter 2. This chapter investigates the CBTD that can be expected from 1) "today's" typical production-line M256 barrels, and 2) an atypical barrel that has the maximum allowable wall thickness variation.

To illustrate the typical case, we have again chosen gun tube serial number 4251, manufactured in September 1987, and described in Chapter 2 (Figures 2 and 3) and Chapter 7 (Table 2). The magnitude of the CBTD will increase with ε and decrease with D. One of the largest ε's and smallest D's for this barrel occurs at z = 4.45 m, where ε = 0.1 mm and D = 22.65 mm. To assess the greatest CBTD buildup that could be expected to occur at this location, we have chosen the worst-case firing scenario used in Gerber and Bundy (1992) and enumerated in Table 3. The firing sequence represents (approximately) the case where all rounds in the M1A1 tank are fired as fast as possible. Figure 14 shows the computed CBTD at this location for the firing scenario of Table 3. It can be seen that the maximum excursion in CBTD is less than 1.5° C. Such a small temperature change for this worst-case scenario indicates that thermal distortion due to wall thickness variation in this, or any similarly made, barrel will not be a serious problem.

On the other hand, if, on the rare occasion, a gun barrel is manufactured with the maximum allowable wall thickness variation of 1.5 mm (ε = 0.75 mm) at this same location, then the CBTD for the firing scenario of Table 3 would be 7.5 times larger than that shown in

Table 3. Worst Case Firing Scenario

1. 17 rounds at 7 rounds/min
2. 5 minute cool-down
3. 17 rounds at 7 rounds/min
4. 5 minute cool-down
5. 7 rounds at 7 rounds/min
6. Cool-down

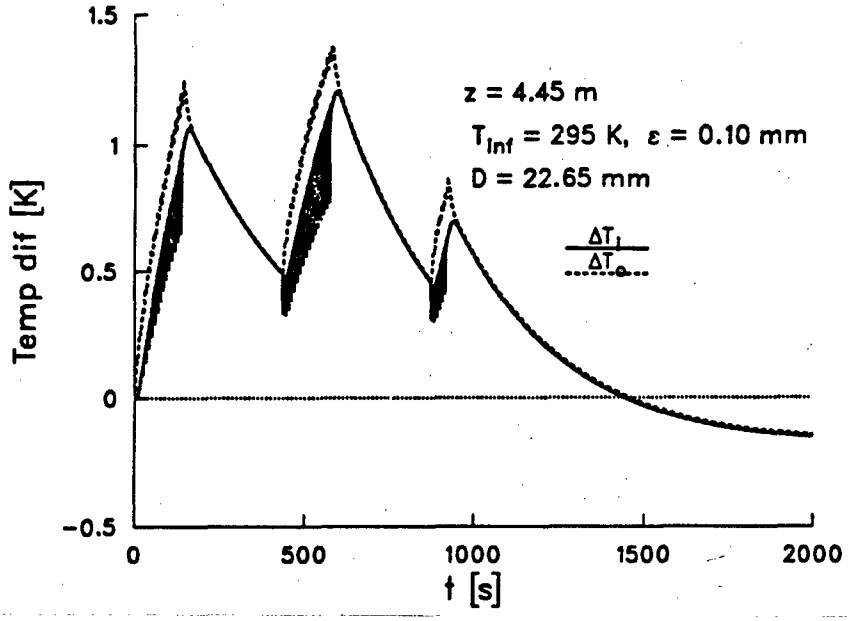

Figure 14. Worst case CBTD for M256 gun barrel, serial number 4251 (typical production line barrel).

Figure 14 (based on the fact that $\Delta T_{o,l}$ is proportional to ε [Equation 17]). In this case, the CBTD would be greater than 10° C, and according to our earlier discussion, the change in muzzle pointing angle would probably exceed 0.5 mrad, noticeably degrading gun accuracy.

In summary, the CBTD that arises during firing due to wall thickness variation is expected to be relatively small for most gun barrels manufactured today. However, the current tolerances would allow a gun barrel to be put into service that could develop a large CBTD during firing and hence, perform poorly from a thermal distortion/gun accuracy standpoint. Thus, consideration should be given to lowering the acceptable wall thickness variation to the same level that most barrels now have, viz., $\varepsilon \leq 0.25$ mm outside the chamber.

INTENTIONALLY LEFT BLANK.

9. REFERENCES

Bundy, M. L. "Thermal Distortion Protection by Candidate Metal and Composite Thermal Shrouds for 120-mm Tank Cannon." BRL-TR-2807, U.S. Army Ballistic Research Laboratory, Aberdeen Proving Ground, MD, June 1987a.

Bundy, M. L. "Analysis of Thermally Induced Barrel Distortion From Firing." Proceedings of the Fifth U.S. Army Symposium on Gun Dynamics, ARCCB-SP-87023, U.S. Army Research, Development and Engineering Center, Close Combat Armament Center, Benet Laboratories, Watervliet, NY, September 1987b.

Chandra, S., and E. B. Fisher. "Simulation of Barrel Heat Transfer." DAAA15-88-D-0014, U.S. Army Ballistic Research Laboratory, Aberdeen Proving Ground, MD, June 1989a.

Chandra, S., and E. B. Fisher. "Analysis of 16-inch/50 Gun Chamber Heating." Veritay Report No. C68-1, Naval Ordnance Station, Indian Head, MD, October 1989b.

Gerber, N., and M. L. Bundy. "Heating of a Tank Gun Barrel: Numerical Study." BRL-MR-3932 (ADA241136), U.S. Army Ballistic Research Laboratory, Aberdeen Proving Ground, MD, August 1991.

Gerber, N., and M. L. Bundy. "Effect of Variable Thermal Properties on Gun Tube Heating." BRL-MR-3984 (ADA253066), U.S. Army Ballistic Research Laboratory, Aberdeen Proving Ground, MD, July 1992.

Gough, P. S. "The NOVA Code: A User's Manual - Volume I. Description and Use." IHCR-80-8, Naval Ordnance Station, Indian Head, MD, December 1980.

Holman, J. P. Heat Transfer. 5th ed., New York: McGraw-Hill Co., p. 6, 1981.

Manaker, A. M., and P. J. Croteau. "Study of Anti-Distortion Jackets." WVT-TR-76028, U.S. Army Benet Weapons Laboratory, Watervliet, NY, July 1976.

McDermott, J. "120-mm M256 Tube, Finished Machined, Dwg. No. 12528311." Sheet 1, rev. W, Procurement and Contracting Directorate, Watervliet Arsenal, NY, June 1991.

Overocker, B. Private communication. Production Planning and Control Division, Watervliet Arsenal, NY, September 1991.

Özisik, M. N. Boundary Value Problems in Heat Conduction. New York: Dover Publications, Inc., 1968.

Stratford, B. S., and G. S. Beavers. "The Calculation of the Compressible Turbulent Boundary Layer in Arbitrary Pressure Gradient - A Correlation of Certain Previous Methods." No. 3207, Aeronautical Research Council R&M, 1961.

Talley, J. Q. "Barrel Heating and Chrome Plate Adhesion in the 120-mm M256 Gun Tube." DAAA21-85-C-0389, U.S. Army Armament Research, Development, and Engineering Center, Picatinny Arsenal, NJ, September 1989.

INTENTIONALLY LEFT BLANK.

APPENDIX A:

STATEMENT OF PROBLEMS IN ξ, t VARIABLES

INTENTIONALLY LEFT BLANK.

We repeat the transformation of Equation 14:

$$\zeta(\xi) = \gamma\xi + (1-\gamma)\xi^{\beta} \qquad (0 < \gamma \le 1, \beta > 2) \qquad r = D\zeta + R_l . \tag{A-1}$$

Then

$$d\zeta/d\xi \equiv \zeta' = \gamma + \beta(1-\gamma)\xi^{\beta-1} \qquad d^2\zeta/d\xi^2 \equiv \zeta'' = \beta(\beta-1)(1-\gamma)\xi^{\beta-2}$$

$$\zeta'(0) = \gamma, \qquad \lambda_1 \equiv \zeta'(1) = \gamma + \beta(1-\gamma)$$

$$\lambda_2 \equiv \zeta''(1) = \beta(\beta-1)(1-\gamma). \tag{A-2}$$

We define $f_1(\xi)$ and $f_2(\xi)$:

$$f_1 = 1/(\zeta')^2,$$

$$f_2 = (D/\zeta')/(D\zeta + R_l) - \zeta''/(\zeta')^3. \tag{A-3}$$

The transformed problem for T_1 is

$$\partial T_1/\partial t = (\alpha/D^2)[f_1(\xi)\,\partial^2 T_1/\partial\xi^2 + f_2(\xi)\,\partial T_1/\partial\xi] \equiv G(\xi, t) , \tag{A-4a}$$

$$k\,\partial T_1/\partial\xi - D\,h_g\,\gamma\,T_1 = -Dh_g\,\gamma\,T_g \qquad \xi = 0, t > 0 , \tag{A-4b}$$

$$[k/(D\lambda_1)]\partial T_1/\partial\xi + [h_\infty + 4F\sigma(T_1^m)^3]\,T_1 = h_\infty T_\infty + F\sigma[T_\infty^4 + 3(T_1^m)^4]$$

$$\xi = 1, \; t > 0 . \tag{A-4c}$$

The transformed problem for T_3 is

$$\partial T_3/\partial t = (\alpha/D^2)[f_1 \ \partial^2 T_3/\partial \xi^2 + f_2 \ \partial T_3/\partial \xi] - (\alpha/r^2)T_3 , \qquad \text{(A-5a)}$$

$$[k/(D\gamma)] \ \partial T_3/\partial \xi - h_g \ T_3 = 0 \qquad \xi = 0, \ t > 0 , \qquad \text{(A-5b)}$$

$$[1/(D\lambda_1)] \ \partial T_3/\partial \xi + (h_\infty + 4F\sigma T_1^3)T_3/k = W(T_1)$$

$$\xi = 1, \ t > 0 , \qquad \text{(A-5c)}$$

where r is given in Equation A-1, λ_1 is given in Equation A-2. T_g and h_g are known functions of t. $W(T_1)$ is defined in Equation 12 and is evaluated in Equation B-11e.

The initial conditions are

$$T_1 = T_\infty \qquad t = 0 , \quad 0 \le \xi \le 1$$

$$T_3 = 0 \qquad t = 0 , \quad 0 \le \xi \le 1. \qquad \text{(A-6)}$$

APPENDIX B:

COEFFICIENTS IN EQUATIONS 20 AND 21

INTENTIONALLY LEFT BLANK.

The following functions of ξ are defined in Equations A-1, A-2, and A-3: ζ, r, ζ', ζ'', f_1, f_2. Also defined are $\gamma = \zeta'(0)$, $\lambda_1 = \zeta'(1)$, $\lambda_2 = \zeta''(1)$. The equations are solved for $t = t^{m+1}$; t^m denotes the preceding time step, when all quantities are known.

Three additional functions of ξ are as follows:

$$g_1 = (\alpha/D^2)\ [f_1/(\Delta\xi)^2 - f_2/(2\,\Delta\xi)],$$

$$g_2 = -(2\,\alpha/D^2)\ f_1/(\Delta\xi)^2,$$

$$g_3 = (\alpha/D^2)\,[f_1/(\Delta\xi)^2 + f_2/(2\,\Delta\xi)]. \qquad \text{(B-1)}$$

The coefficients A_{jn} and d_j in Equation 20 are now given:

$$A_{11} = 3 + 2\,\Delta\xi\ \ D\,\gamma\,h_g/k, \qquad A_{12} = -4, \qquad A_{13} = 1\,, \qquad \text{(B-2)}$$

$$A_{NI+1,\,NI-1} = 1\,, \qquad A_{NI+1,\,NI} = -4$$

$$A_{NI+1,\,NI+1} = 3 + (2\Delta\xi\ D\lambda_1/k)\ [h_\infty + 4F\sigma(T_1^{\,m}{}_{NI+1})^3] \quad at\ r=R_o\,. \qquad \text{(B-3)}$$

For $2 \le j \le NI$,

$$A_{j,j-1} = -\,(\Delta t/2)\ g_1(\xi_j), \qquad \xi_j = (j-1)\,\Delta\xi$$

$$A_{j,j} = 1 - (\Delta t/2)\ g_2(\xi_j), \qquad A_{j,j+1} = -\,(\Delta t/2)\ g_3(\xi_j)\,. \qquad \text{(B-4)}$$

All other coefficients A_{jn} are equal to zero.

$$d_1 = 2\,\Delta\xi\, D\,\gamma\, h_g T_g / k,$$

$$d_{NI+1} = (2\,\Delta\xi\, D\lambda_1/k)\left[h_\infty T_\infty + F\sigma\left\{T_\infty^4 + 3\left(T_{1\,NI+1}^{m}\right)^4\right\}\right]. \qquad \text{(B-5)}$$

For $2 \le j \le NI$,

$$d_j = T_{1_j}^{m} + (\Delta t/2)\, G_j^m, \qquad \text{(B-6a)}$$

where

$$G_j^m = g_1(\xi_j)\;\; T_{1_{j-1}}^{m} + g_2(\xi_j)\; T_{1_j}^{m} + g_3(\xi_j)\; T_{1_{j+1}}^{m}. \qquad \text{(B-6b)}$$

Now the coefficients B_{jn} and e_j in Equation 21 are given:

$$B_{11} = A_{11}, \qquad B_{12} = A_{12}, \qquad B_{13} = A_{13}, \qquad \text{(B-7)}$$

$$B_{NI+1,NI-1} = 1, \quad B_{NI+1,NI} = -4,$$

$$B_{NI+1,NI+1} = 3 + (2\,\Delta\xi\, D\lambda_1/k)\left[h_\infty + 4F\sigma\left(T_{1\,NI+1}^{m+1}\right)^3\right]. \qquad \text{(B-8)}$$

For $2 \le j \le NI$,

$$B_{j,j-1} = A_{j,j-1}, \qquad B_{j,j} = A_{j,j} + (\alpha\,\Delta\, t/2)/r_j^2, \qquad B_{j,j+1} = A_{j,j+1}. \qquad \text{(B-9)}$$

All other coefficients B_{jn} are equal to zero.

$$e_1 = 0, \qquad e_{NI+1} = 2\,D\lambda_1\,\Delta\xi\; W\left(T_{1\,NI+1}^{m+1}\right), \qquad \text{(B-10)}$$

where $W(T_{1_{NI+1}}^{m+1})$, defined in Equation 12, is approximated by the following sequence, evaluated at $t = t^{m+1}$, where r and ξ subscripts denote partial differentiation:

$$k T_{1_r}(\xi=1) = h_\infty T_\infty + F\sigma[T_\infty^4 + 3(T_{1_{NI+1}}^m)^4] - [h_\infty + 4F\sigma(T_{1_{NI+1}}^m)^3] T_{1_{NI+1}}^{m+1}, \quad \text{(B-11a)}$$

$$T_{1_\xi}(\xi=1) = D\lambda_1 T_{1_r}(\xi=1), \quad \text{(B-11b)}$$

$$T_{1_{\xi\xi}}(1) = [1/\{2(\Delta\xi)^2\}][8T_{1_{NI}} - T_{1_{NI-1}} - 7T_{1_{NI+1}}] + (3/\Delta\xi)\, T_{1_\xi}(1), \quad \text{(B-11c)}$$

$$T_{1_\pi}(1) = (1/D)^2[(1/\lambda_1^2) T_{1_{\xi\xi}}(1) - (\lambda_2/\lambda_1^3) T_{1_\xi}(1)], \quad \text{(B-11d)}$$

$$W(T_{1_{NI+1}}^{m+1}) = -T_{1_\pi}(1) - [h_\infty + 4F\sigma(T_{1_{NI+1}}^{m+1})^3] T_{1_r}(1)/k. \quad \text{(B-11e)}$$

For $2 \le j \le NI$,

$$e_j = T_{3_j}^m + (\Delta t/2)\bar{G}_j^m - (\Delta t/2)\,(\alpha/r_j^2) T_{3_j}^m, \quad \text{(B-12)}$$

where

$$\bar{G}_j^m = g_1(\xi_j)\, T_{3_{j-1}}^m + g_2(\xi_j) T_{3_j}^m + g_3(\xi_j) T_{3_{j+1}}^m. \quad \text{(B-13)}$$

INTENTIONALLY LEFT BLANK.

APPENDIX C:

TIME SCALE

INTENTIONALLY LEFT BLANK.

Here, time = t' will refer to time within one firing cycle; $t' = 0$ at the beginning of the cycle. Six constants are given: t_d, t_f, t'_1, t'_2, $\Delta t'_1$, and $\Delta t'_2$. Here, t_d is the delay time for the rapid rise in T_g and h_g from initial conditions, and t_f is the time between successive firings. The time increment Δt (t') is given by the following function:

$$\begin{aligned} \Delta t &= t_d - \Delta t'_1 && 0 \le t' < t_d - \Delta t'_1 \\ \Delta t &= \Delta t'_1 && t_d - \Delta t'_1 \le t' < t'_1 \\ \Delta t &= C_1 + C_2 t' && t'_1 \le t' < t'_2 \\ \Delta t &= \Delta t'_2 && t'_2 \le t', \end{aligned}$$

where

$$C_2 = (\Delta t'_2 - \Delta t'_1)/(t'_2 - t'_1) \text{ and } C_1 = \Delta t'_2 - C_2\, t'_2$$

(If $t' + \Delta t'_2 > t_f$, set $\Delta t = t_f - t'$).

A typical set of values of the parameters would be the following:

$$t'_1 = 0.018 \text{ s}, \quad t'_2 = 10.0 \text{ s}, \quad \Delta t'_1 = 0.00025 \text{ s}, \quad \Delta t'_2 = 6.0 \text{ s}.$$

INTENTIONALLY LEFT BLANK.

APPENDIX D:

ANALYTICAL MODEL OF COOLING

INTENTIONALLY LEFT BLANK.

The coalescence of the inner and outer wall cooling curves in Figures 5, 7, and 12 suggest that temperature may be approximated at fixed z by the following expression after radial equilibration in T_1 and T_3 is attained:

$$T = \bar{T}_1(t) + (\varepsilon \cos\phi)\,\bar{T}_3(t)\,, \qquad \text{(D-1)}$$

where $\bar{T}_1$ and $\bar{T}_3$ are T_1 and T_3 values for $t > t_r$, t_{r3} that are constant at this time. We consider a control volume of unit axial length and a quadrant cross-section bounded by: (1) $r = R_i$; (2) $r = r_o = R_o + \varepsilon \cos\phi$; (3) $\phi = 0$; (4) $\phi = \pi/2$. We shall retain terms only through $O(\varepsilon)$. In addition, we assume

$$T_g = T_\infty, \qquad h_g = h_\infty. \qquad \text{(D-2)}$$

The rate of change of heat energy in the control volume is

$$\dot{H}_b = \int_0^{\pi/2} \int_{R_i}^{R_o + \varepsilon\cos\phi} \rho c_p (dT/dt)\, r\, dr\, d\phi \qquad J/s. \qquad \text{(D-3)}$$

Heat flux through the inner wall is

$$\dot{H}_i = \int_0^{\pi/2} h_g (T_\infty - T)\, R_i\, d\phi \qquad J/s. \qquad \text{(D-4)}$$

Heat flux through the outer wall, neglecting radiation, is

$$\dot{H}_o = \int_0^{\pi/2} h_\infty (T_\infty - T)(R_o + \varepsilon\cos\phi)\, d\phi \qquad J/s. \qquad \text{(D-5)}$$

There is no heat flow across $\phi = 0$ because of the physical symmetry in the problem. The heat flow rate across the plane $\phi = \pi/2$ is

$$\dot{H}_\phi = \int_{R_i}^{R_o + \varepsilon\cos\phi} (k/r)(\partial T/\partial\phi)_{\phi = \pi/2}\, dr \qquad J/s. \qquad \text{(D-6)}$$

The energy balance equation is

$$\dot{H}_b = \dot{H}_i + \dot{H}_o + \dot{H}_\phi \ . \qquad \text{(D-7)}$$

Equation D-1 is substituted into Equations D-3, D-4, D-5, and D-6. When these equations are substituted into Equation D-7, and coefficients of like powers of ε are collected, we obtain linear first-order ordinary differential equations for $\bar{T}_1$ and $\bar{T}_3$. The solution is

$$\bar{T}_1 = T_\infty + [T_1(t_a) - T_\infty]\, exp[-c_1(t - t_a)] \ , \qquad \text{(D-8a)}$$

$$\bar{T}_3 = c_2\, exp[-c_1(t - t_a)] + [T_3(t_a) - c_2]\, exp[-c_3(t - t_a)] \ , \qquad \text{(D-8b)}$$

where

$$c_1 = 2\,h_\infty/[\rho\, c_p(R_o - R_i)] \ , \qquad \text{(D-9a)}$$

$$c_2 = (h_\infty/k)\,(R_o + R_i)\,[T_1(t_a) - T_\infty]/[(R_o - R_i)\,ln(R_o/R_i)] \ , \qquad \text{(D-9b)}$$

$$c_3 = c_1 + [2\,k\,ln\,(R_o/R_i)]/[\rho\, c_p(R_o^2 - R_i^2)] \ . \qquad \text{(D-9c)}$$

The quantities $T_1\,(t_a)$ and $T_3\,(t_a)$ are finite-difference results for $r = R_o$ at a time $t = t_a\ (> t_r, t_{r3})$, chosen so that $T_3\,(t_a) < 0$ (or $\Delta T_o > 0$). The time of undershoot, t_u, is found by setting $\bar{T}_3$ in Equation D-8b equal to zero:

$$t_u = t_a + [\rho\, c_p(R_o^2 - R_i^2)/\{2\,k\,ln\,(R_o/R_i)\}]$$
$$\times\, ln\left[1 - \frac{T_3(t_a)\,k}{h_\infty}\,\frac{(R_o - R_i)\,ln\,(R_o/R_i)}{(R_o + R_i)\,\{T_1(t_a) - T_\infty\}}\right]. \qquad \text{(D-10)}$$

As an example, assume a scenario in which five rounds are fired 120 seconds apart before the final cooling starts. In this case, Equation D-8 would predict ΔT_o as shown in Figure D-1. The agreement between analytical and numerical solutions for ΔT_o ($\approx -2\varepsilon\ T_3\ (R_o)$) is very good.

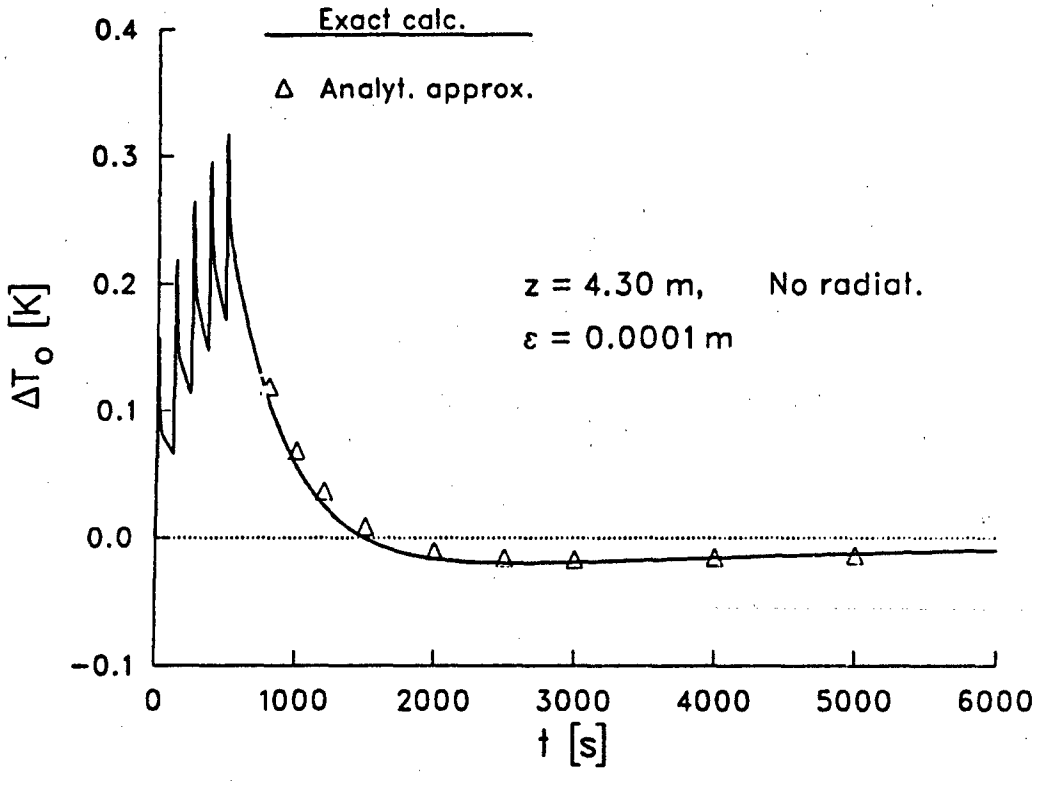

Figure D-1. Comparison of ΔT_o cooling histories for analytical model and numerical output (t_o = 1,000 s).

INTENTIONALLY LEFT BLANK.

LIST OF SYMBOLS

A_{jn}, B_{jn}	coefficients in linear equations for T_1 and T_3, Equations 20 and 21
c_p	specific heat of gun barrel (Joules/[kg K])
c_1, c_2, c_3	constants defined in Equations D-9
CBTD	cross-barrel temperature difference
d_j, e_j	coefficients in linear equations for T_1 and T_3, right-hand sides of Equations 20 and 21
D	$= R_o - R_i$ [m, mm]
f_1, f_2	given functions of ξ, Equation A-3
F	radiation interchange factor, Equation 6
g_1, g_2, g_3	functions of ξ, defined in Equation B-1
$G(\xi,t)$	function of ξ and t, defined in Equations A-4a and B-6
$\bar{G}(\xi, t)$	function of ξ and t, defined in Equation B-13
$h_g(t, z)$	heat transfer coefficient - bore gas to gun barrel (Joules/{m^2 s K})
$h_\infty(z)$	heat transfer coefficient - gun barrel to ambient air (Joules/{m^2 s K})
j	subscript index indicating radial location of a nodal point
k	thermal conductivity of gun barrel (Joules/{m s K})
m	superscript index indicating time value
n	arc length along line normal to the surface of the outer wall
NI	number of intervals in $R_i \le r \le R_o$ formed by the nodal points
r	radial coordinate in transverse plane [m, mm] ($r = 0$ at axis of gun bore)
r'	radial coordinate in transverse plane ($r' = 0$ at axis of outer wall)
r_o	$= r_o(\phi)$ = radial coordinate of outer wall $= R_o + \varepsilon \cos\phi$
R_i	radius of circular inner wall [m, mm]

R_o	radius of circular outer wall [m, mm]
t	time from initiation of first round [s, ms, min]
t_a	initial time for analytical model, Equations D-8 [s]
t_d	delay time at given z for rapid rise in T_g and h_g [s, ms]
t_f	time interval between successive rounds
t_r	rise time for T_1 [s, ms]
t_{r3}	rise time for T_3 [s, ms]
t_u	time at which ΔT_o changes sign, Equation D-10 [s]
t'	time measured within a firing cycle [s, ms]
t_1' , t_2'	two prescribed time values in Timescale formula, Appendix C [s]
T	temperature in the gun barrel [K]
T_g	$= T_g(t)$ = temperature in the bore at a fixed z-value [K]
T_i , T_o	temperatures at inner and outer walls, respectively, of gun barrel [K], Equations 15 and 16
T_1	axisymmetric contribution to barrel temperature, Equation 9 [K]
T_3	function furnishing non-axisymmetric contribution to barrel temperature, Equation 9 [K/m]
$\bar{T}_1$, $\bar{T}_3$	analytical approximation to T_1 and T_3, respectively, Equation D-1
T_∞, T_{inf}	temperature in ambient air [K]
$\underline{U}_n$	unit vector normal to the outer wall
$W(T_1)$	function of T_1 defined in Equation 12, evaluated in Appendix B
z	axial coordinate ($z = 0$ at breech) [m]
α	$= k/(\rho\, c_p)$ = thermal diffusivity of gun barrel [m^2/s]
β, γ	prescribed constants in transformation formula, Equation 14
Δt	time increment for calculation of temperature profile, Equation 19 [s]

$\Delta t_1'$, $\Delta t_2'$	two prescribed time increments in the Timescale formula, Appendix C [s]
ΔT_I	temperature difference between points x_2 and x_1 in Figure 1, see Equation 17a
ΔT_o	temperature difference between points x_4 and x_3 in Figure 1 see Equation 17b
$\Delta\xi$	constant increment in ξ in range $0 \le \xi \le 1$; $\Delta\xi = 1/NI$
ε	distance between the centers of the inner and outer walls of a gun barrel [m]
ζ	transformation variable, given in Equation 14, also Equation A-1
λ_1, λ_2	$= \zeta'(1), \zeta''(1)$ - - constants defined in Equation A-2
ξ	transformed radial variable, Equations 13 and 14, also Equation A-1
ρ	density of gun barrel metal [kg/m^3]
σ	Stefan-Boltzmann constant = 5.669×10^{-8} J/(m^2 s K^4)
ϕ	azimuthal coordinate in transverse plane
ϕ'	azimuthal coordinate in transverse plane relative to origin at center of outer wall (Figure 1b)

INTENTIONALLY LEFT BLANK.

No. of Copies | Organization

2 Administrator
Defense Technical Info Center
ATTN: DTIC-DDA
Cameron Station
Alexandria, VA 22304-6145

1 Commander
U.S. Army Materiel Command
ATTN: AMCAM
5001 Eisenhower Ave.
Alexandria, VA 22333-0001

1 Director
U.S. Army Research Laboratory
ATTN: AMSRL-D
2800 Powder Mill Rd.
Adelphi, MD 20783-1145

1 Director
U.S. Army Research Laboratory
ATTN: AMSRL-OP-CI-AD,
Tech Publishing
2800 Powder Mill Rd.
Adelphi, MD 20783-1145

2 Commander
U.S. Army Armament Research,
Development, and Engineering Center
ATTN: SMCAR-IMI-I
Picatinny Arsenal, NJ 07806-5000

2 Commander
U.S. Army Armament Research,
Development, and Engineering Center
ATTN: SMCAR-TDC
Picatinny Arsenal, NJ 07806-5000

1 Director
Benet Weapons Laboratory
U.S. Army Armament Research,
Development, and Engineering Center
ATTN: SMCAR-CCB-TL
Watervliet, NY 12189-4050

(Unclass. only)1 Commander
U.S. Army Rock Island Arsenal
ATTN: SMCRI-IMC-RT/Technical Library
Rock Island, IL 61299-5000

1 Director
U.S. Army Aviation Research
and Technology Activity
ATTN: SAVRT-R (Library)
M/S 219-3
Ames Research Center
Moffett Field, CA 94035-1000

No. of Copies | Organization

1 Commander
U.S. Army Missile Command
ATTN: AMSMI-RD-CS-R (DOC)
Redstone Arsenal, AL 35898-5010

1 Commander
U.S. Army Tank-Automotive Command
ATTN: ASQNC-TAC-DIT (Technical
Information Center)
Warren, MI 48397-5000

1 Director
U.S. Army TRADOC Analysis Command
ATTN: ATRC-WSR
White Sands Missile Range, NM 88002-5502

1 Commandant
U.S. Army Field Artillery School
ATTN: ATSF-CSI
Ft. Sill, OK 73503-5000

(Class. only)1 Commandant
U.S. Army Infantry School
ATTN: ATSH-CD (Security Mgr.)
Fort Benning, GA 31905-5660

(Unclass. only)1 Commandant
U.S. Army Infantry School
ATTN: ATSH-CD-CSO-OR
Fort Benning, GA 31905-5660

1 WL/MNOI
Eglin AFB, FL 32542-5000

Aberdeen Proving Ground

2 Dir, USAMSAA
ATTN: AMXSY-D
AMXSY-MP, H. Cohen

1 Cdr, USATECOM
ATTN: AMSTE-TC

1 Dir, ERDEC
ATTN: SCBRD-RT

1 Cdr, CBDA
ATTN: AMSCB-CI

1 Dir, USARL
ATTN: AMSRL-SL-I

10 Dir, USARL
ATTN: AMSRL-OP-CI-B (Tech Lib)

No. of
Copies Organization

16 Director
Benet Weapons Laboratory
U.S. Army Armament Research,
Development, and Engineering Center
ATTN: SMCAR-CCB-DS, R. Hasenbein
SMCAR-CCB-DA,
J. Neice
G. Carafano
SMCAR-CCB-RA,
B. Pflegl
P. O'Hara
SMCAR-CCB-RT,
B. Avitzar
S. Sopok
SMCAR-CCB-RM, M. Withesell
SMCAR-CCB-DI, C. Rinaldi
SMCAR-CCB-RP,
J. Cox
G. Capsinalis
SMCAR-CCB-DS, P. Votlis
SMCAR-CCB-DS, C. Andrade
SMCAR-LBD-D, J. Zweig
SMCAR-CCB, L. Johnson
SMCAR-CCB-DA, L. Bennett
Watervliet, NY 12189-4050

2 Director
Benet Weapons Laboratory
U.S. Army Armament Research,
Development, and Engineering Center
ATTN: T. Allen
B. Artus
Watervliet, NY 12189-4050

1 Commander
U.S. Army Tank-Automotive Command
ATTN: SFAE-ASM-AB-SW, Dr. Pattison
Warren, MI 48397-5000

5 Commander
Tank Main Armament System
ATTN: SFAE-AR-TMA,
K. Russell
E. Kopacz
K. Ruben
F. Hildebrand
S. Bernstein
Picatinny Arsenal, NJ 07806-5000

No. of
Copies Organization

2 Commander
U.S. Army Armament Research,
Development, and Engineering Center
ATTN: SMCAR-CCH,
E. Del Coco
K. Pfleger
Picatinny Arsenal, NJ 07806-5000

2 Commander
U.S. Army Armament Research,
Development, and Engineering Center
ATTN: C. Langon
J. Delabar
Picatinny Arsenal, NJ 07806-5000

1 Director
Weapons Department
U.S. Army Armor School
ATTN: ATSB-WP-ORSA, A. Pomey
Fort Knox, KY 40121-5212

1 Paul Gough Associates, Inc.
ATTN: Dr. Paul S. Gough
1048 South St.
Portsmouth, NH 03801-5423

2 Veritay Technology Incorporated
ATTN: E. B. Fisher
J. Z. Talley
P.O. Box 305
4845 Millersport Highway
East Amhurst, NY 14051

USER EVALUATION SHEET/CHANGE OF ADDRESS

This Laboratory undertakes a continuing effort to improve the quality of the reports it publishes. Your comments/answers to the items/questions below will aid us in our efforts.

1. ARL Report Number ARL-TR-100 Date of Report March 1993

2. Date Report Received _____

3. Does this report satisfy a need? (Comment on purpose, related project, or other area of interest for which the report will be used.) _____

4. Specifically, how is the report being used? (Information source, design data, procedure, source of ideas, etc.) _____

5. Has the information in this report led to any quantitative savings as far as man-hours or dollars saved, operating costs avoided, or efficiencies achieved, etc? If so, please elaborate. _____

6. General Comments. What do you think should be changed to improve future reports? (Indicate changes to organization, technical content, format, etc.) _____

CURRENT ADDRESS

_____
Organization

_____
Name

_____
Street or P.O. Box No.

_____
City, State, Zip Code

7. If indicating a Change of Address or Address Correction, please provide the Current or Correct address above and the Old or Incorrect address below.

OLD ADDRESS

_____
Organization

_____
Name

_____
Street or P.O. Box No.

_____
City, State, Zip Code

(Remove this sheet, fold as indicated, staple or tape closed, and mail.)

DEPARTMENT OF THE ARMY

OFFICIAL BUSINESS

BUSINESS REPLY MAIL
FIRST CLASS PERMIT No 0001, APG, MD

Postage will be paid by addressee

Director
U.S. Army Research Laboratory
ATTN: AMSRL-OP-CI-B (Tech Lib)
Aberdeen Proving Ground, MD 21005-5066

NO POSTAGE
NECESSARY
IF MAILED
IN THE
UNITED STATES